Fracture Mechanics of Concrete Structures, de Borst et al (eds) © 2001 Swets & Zeitlinger, Lisse, ISBN 90 2651 825 0

Size effect analysis of reinforced concrete deep beams

T.Hasegawa
Institute of Technology, Shimizu Corporation, Tokyo, Japan

ABSTRACT: A finite element failure analysis of reinforced concrete deep beams is performed using the Multi Equivalent Series Phase Model and the Enhanced Microplane Concrete Model to simulate experimentally obtained size effects of the deep beams. It is shown that the models can provide good prediction of experimental results of reinforced concrete deep beams on the cracking, shear-compressive failure localization, failure mechanism, deformation, shear strength, and its size effect. The loading boundary condition and the geometrical unsimilarity in beam shape other than in the shear span are shown to have important influence on not only the shear strength but also the failure mode and post-peak behavior.

1 INTRODUCTION

Comparing with reinforced concrete slender beams, fracture and size effect in reinforced concrete deep beams are complicatedly influenced by a lot of factors like the formation of failure mechanism by crack propagation, size effects in tensile fracture, localized shear-compressive failure, and so on. Therefore, a numerical simulation of the failure mechanism in reinforced concrete deep beams is important to establish a rational shear design method for them.

In the present study, a general purpose finite element system DIANA incorporating the nonlocal Multi Equivalent Series Phase Model (MESP Model; Hasegawa 1998) and the local Enhanced Microplane Concrete Model (EMPC Model; Hasegawa 1995) is utilized to simulate size effect tests of reinforced concrete deep beams of Niwa (Niwa 1983) and Matsuo (Matsuo 2001). The MESP Model (Figure 1) as a nonlocal constitutive law for concrete has been demonstrated to be able to predict size effects in tensile fractures, multiaxial compressive failures, and shear fractures of concrete, which is suitable for simulating failures of reinforced concrete deep beams under the complicated stress condition.

2 ANALYSIS MODELING

2.1 *Analysis cases A, B, and C*

Shear tests of three reinforced concrete deep beam specimens of Niwa are simulated in the first series of the analysis cases A, B, and C. Those specimens called SI0, SI1, and LR0 have the same $a/d = 0.5$ (a = shear span length; d = effective depth), but individual d of 300, 600, and 900 mm, respectively. The specimens are not geometrically similar, but only effective depth and shear span length are similar among the three specimens. The finite element mesh used in each analysis case is shown in Figures 2-6. Assuming symmetry of the structure, only half-left structure models are considered. In the analysis cases A and C, the finite elements in the web plain concrete portion are enlarged similarly to discretize the three test specimens with different sizes into individual finite element meshes. The nonlocal MESP Model is used for the plain concrete portions of the specimens in the analysis case A. On the other hand, the local EMPC Model is applied to the same concrete portion in the analysis case C to compare the results of the analysis cases A and C and investigate the effectiveness of the nonlocal constitutive model. In the analysis case B, the finite element size in the web concrete portion of the smallest specimen are kept constant to discretize the other two larger specimens. The MESP Model is used in the analysis case B to examine mesh dependency of the model.

2.2 *Analysis cases D, E, and F*

In the second series of the analysis cases D, E, and F shear tests of three reinforced concrete deep beam specimens of Matsuo are simulated. Those specimens called D200, D400, and D600 have the same $a/d = 1.0$, but individual d of 200, 400, and 600 mm, respectively. As in the experiment of Niwa, the specimens of Matsuo are not geometrically similar, but only effective depth and shear span length are similar among the three specimens. The finite element mesh used in each analysis case is shown in Figures 7-10. In the analysis case D the finite

elements in the web concrete portion are enlarged similarly to discretize the test specimens into finite element meshes, as in the analysis cases A and C. The MESP Model is used for the plain concrete portions of the specimens in the analysis case D.

In the analysis case E the specimen D600 is discretized as a full structure model, not exploiting its symmetry. Furthermore, in the analysis case F to examine the influence of rotation and deformation of loading plate, the fixed displacement load is applied to only a single central node of loading plate elements.

2.3 *Tension stiffening model*

In all the cases, reinforcement bars are modeled with the embedded reinforcement elements of Von Mises elasto-plastic constitutive model taking into account tension stiffening effect of concrete. The elements within the 100 mm height around the tension reinforcement bar are assumed as bond concrete elements to take into account tension stiffening effect of concrete. The local EMPC Model is assumed for the bond concrete. Figure 11 shows the uniaxial response of the local EMPC Model for the tension stiffening in the bond concrete elements comparing with experimental data (Shima et al. 1987).

2.4 *Regularization with MESP Model*

In the MESP Model, fracture localization at the microscopic level is modeled using a series phase consisting of fracture and unloading phases. Through a simple homogenization procedure for the individual series phase, the characteristics on orientation and size of series phases in the concrete volume element are taken into account in the resulting nonlocal macroscopic constitutive relation of the MESP Model (Figure 1). This yields a regularization of the MESP Model. Assuming the length l^F of the fracture phase as $2l^F = d_{\max}$, the material parameters of the EMPC and MESP Models are determined by fitting the uniaxial tension softening relation to the one provided in CEB-FIP Model Code 1990 ($d_{\max}$ = the maximum aggregate size). Then the regularization of the MESP Model for the individual finite element is achieved by taking into account the lengths of series phases in the element to calculate incremental stiffness of the model. Figures 12 and 13 show size effects of the MESP Model on the uniaxial tension and

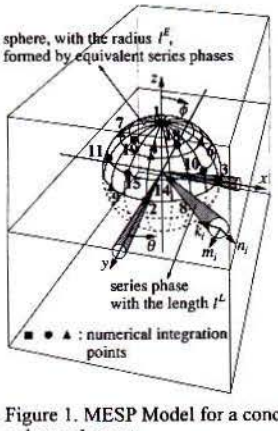

Figure 1. MESP Model for a concrete volume element

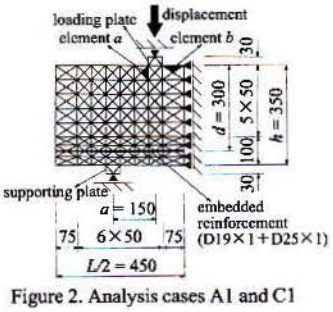

Figure 2. Analysis cases A1 and C1

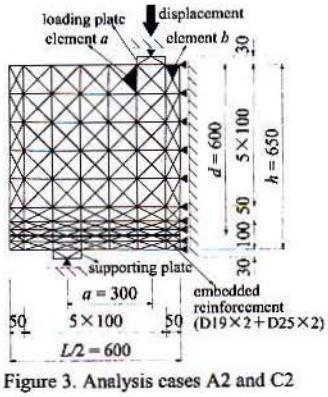

Figure 3. Analysis cases A2 and C2

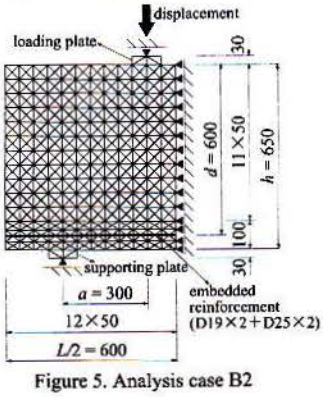

Figure 5. Analysis case B2

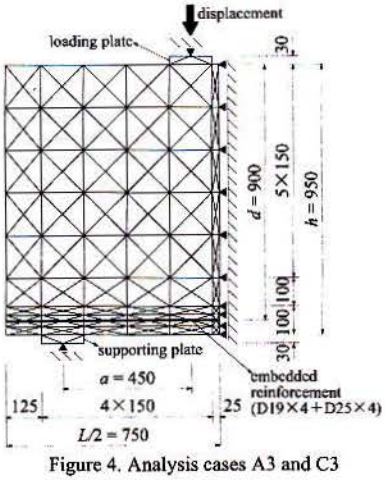

Figure 4. Analysis cases A3 and C3

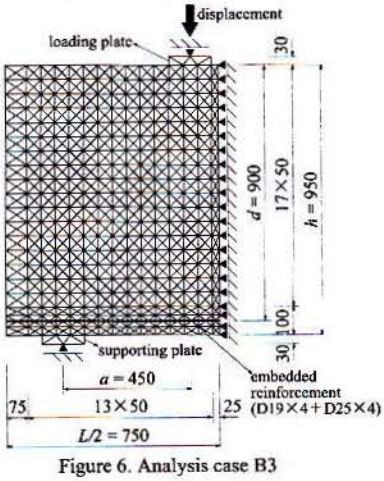

Figure 6. Analysis case B3

compression for the concrete triangle elements used in the present analysis. The size effects result from the regularization with the MESP Model.

3 ANALYSIS RESULTS AND DISCUSSION

3.1 *Analysis cases A, B, and C*

The size effect of shear strength obtained in each analysis case is shown in Figure 14 along with experimental test data of Niwa, in which $\tau_u = V_u/bd$ = shear strength; V_u = maximum shear load; b = beam width; f_c' = concrete compressive strength. The design equation of the Japan Society of Civil Engineers Standard Specification is compared with the size effect in the same figure. Three analysis cases provide reasonable size effects of the shear strength.

The size effect obtained in the analysis case A using the similar elements resembles the one obtained in the analysis case B using the elements with the same size. The maximum difference of the shear strength between the two analysis cases is about 10%. The MESP Model relieves mesh dependency. It is worth notice that the EMPC Model (the analysis case C) also can predict an adequate size effect in spite of a local constitutive model. This is because there was an apparent size effect in the tests of Niwa due to the

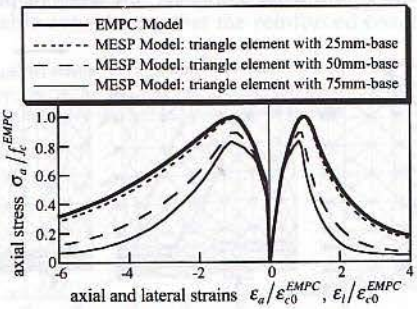

Figure 13. Uniaxial compression

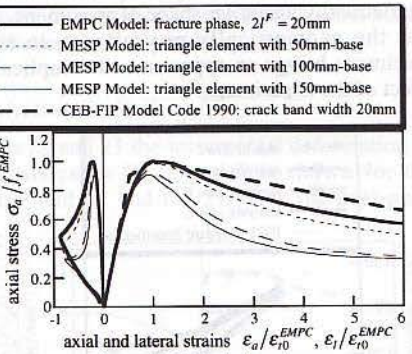

Figure 12. Uniaxial tension

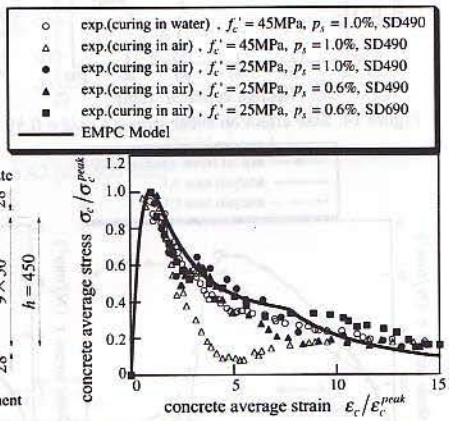

Figure 11. Tension stiffening

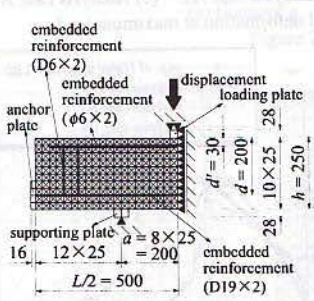

Figure 7. Analysis case D1

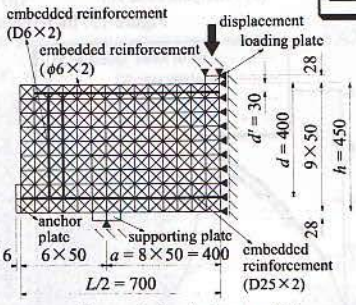

Figure 8. Analysis case D2

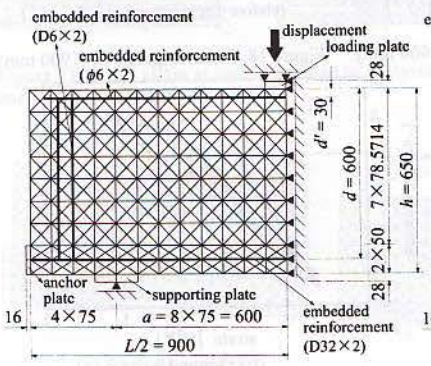

Figure 9. Analysis case D3

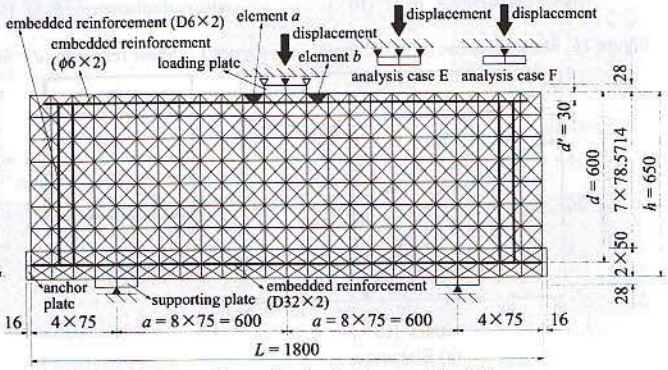

Figure 10. Analysis cases E and F

geometrically unsimilar shape of test specimens and the size effect of failure mode.

In Figure 15 the incremental deformation at the maximum load in the analysis case A is compared for three specimens having the different effective depth. All specimens collapse due to the shear-compressive failure localization near the loading plate. However, the position of the element failing in the shear-compressive softening localization is different among the three specimens, which means that the failure mode depends on the specimen size due to the geometrically unsimilar shape of specimens. It seems that the geometrically unsimilarity in shape of specimens brings an apparent and complicated size effect of the experiment.

In the previous studies (Hasegawa 1999, Yoshitake & Hasegawa 2000) it has been clarified that only tensile modeling which takes into account fracture energy is not sufficient to simulate the size effect of shear strength of reinforced concrete deep beams having the completely similar shape. It has been concluded that some models for the size effect on shear-compressive failure of concrete like the MESP Model are necessary for the simulation and the geometrical unsimilarity in beam shape results in the apparent size effect in the experiment of Niwa.

Figures 16-18 are the shear responses in each analysis case comparing with the experiment, in which shear stress $\tau = V/bd$; V = shear load; δ_P = relative displacement between the loading and supporting plates. Both the MESP and EMPC Models provide good prediction of the shear response up to the maximum load. However, the analysis predicts

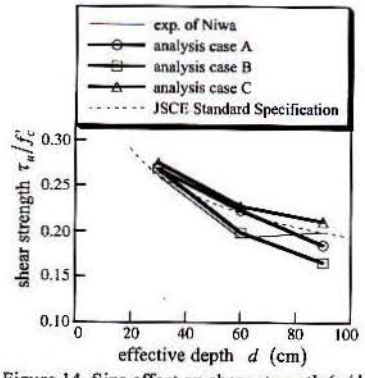

Figure 14. Size effect on shear strength (a/d = 0.5)

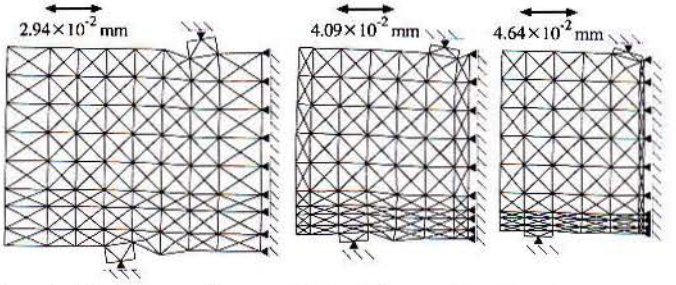

(a) Analysis case A1 (b) Analysis case A2 (c) Analysis case A3

Figure 15. Incremental deformation at maximum load

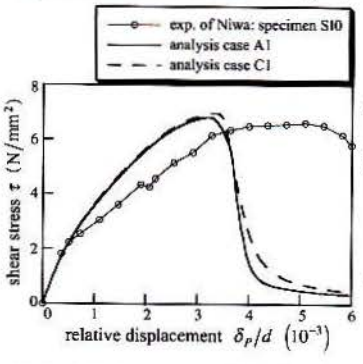

Figure 16. Shear response (d = 300 mm)

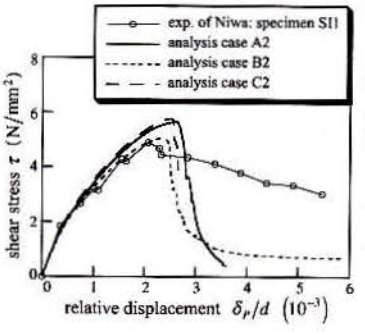

Figure 17. Shear response (d = 600 mm)

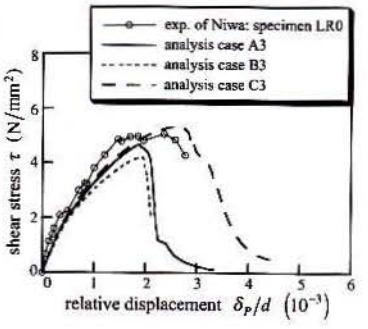

Figure 18. Shear response (d = 900 mm)

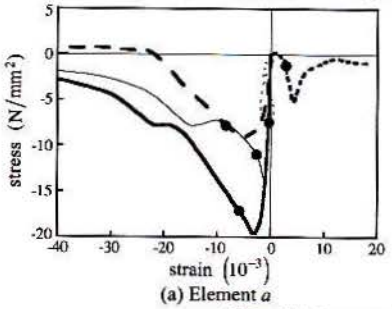

(a) Element a

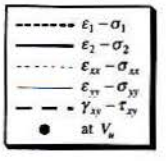

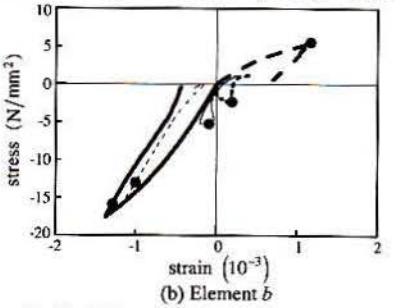

(b) Element b

Figure 19. Stress-strain responses in analysis case A1 (d = 300 mm)

very brittle responses in the post-peak regime while the experiment shows relatively ductile post-peak behavior. This might be due to insufficient regularization for compression in the analysis, and some problems related to analytical modeling of the loading boundary condition in the experiment.

Figures 19 and 20 show the stress-strain responses of the elements *a* and *b* (Figures 2 and 3) in the analysis cases A1 (d = 300 mm) and A2 (d = 600 mm). In the smaller specimen (d = 300 mm) the shear-compressive softening failure occurs at the element *a* within the shear span and the unloading takes place at the element *b* outside the shear span. On the other hand in the larger specimen (d = 600 mm), the shear-compressive softening failure localizes at the element *b* outside the shear span and the unloading occurs at the element *a* within the shear span. The brittle post-peak shear response obtained in the analysis is reasonable considering that the reinforced concrete deep beam failed in the shear-compressive softening localization and the unloading is dominant outside of the localization area.

In Figure 21 plotted is the line of maximum principal strain $\varepsilon_1 \geq 5\varepsilon_{t0}$ with the thickness proportional to its value to represent crack strain and crack direction at the maximum load in the analysis cases A3 and B3, which will be a good measure of crack width (ε_{t0} = the tensile strain corresponding to tensile strength). Similar cracking patterns are obtained in the analysis cases A3 with coarse mesh and B3 with fine mesh, which means that the MESP Model relieves mesh dependency on cracking.

3.2 *Analysis cases D, E, and F*

In Figures 22 and 23 the incremental deformation of the analysis cases D, E, and F is shown for the maximum load V_u and for $2V_u/3$ in the post-peak

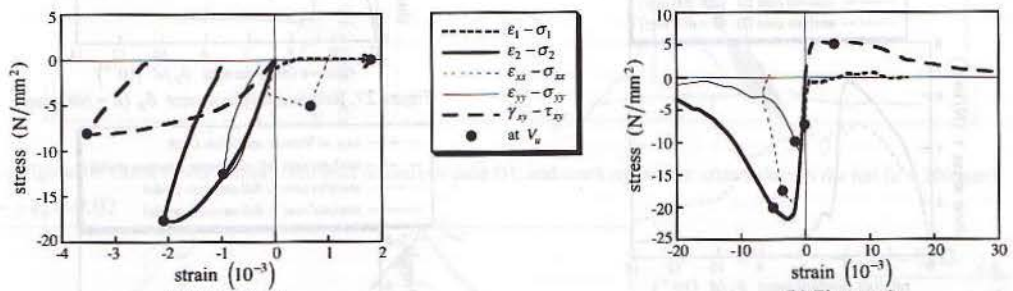

(a) Element *a* (b) Element *b*

Figure 20. Stress-strain responses in analysis case A2 (d = 600 mm)

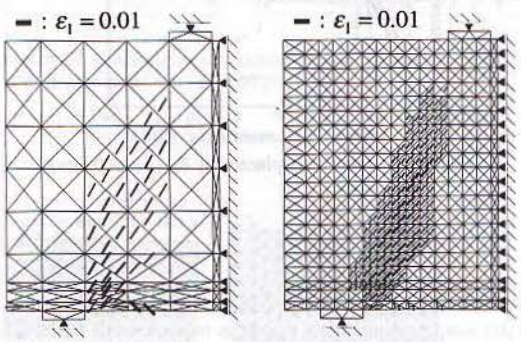

Figure 21. Crack strain at maximum load in analysis cases A3 and B3 (d = 900 mm)

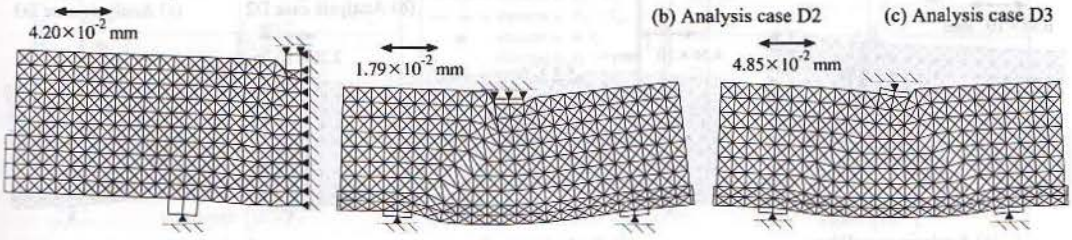

(a) Analysis case D1 (d) Analysis case E (e) Analysis case F

(b) Analysis case D2 (c) Analysis case D3

Figure 22. Incremental deformation at maximum load

regime. Figure 24 is the shear responses of the analysis cases D1 (d = 200 mm) and D2 (d = 400 mm) in terms of the relative displacement δ_R of the center point of beam to the supporting point at the level of tension reinforcement bar comparing to the experiment. On the other hand Figure 25 is the shear responses of the analysis cases D1 and D2 in terms of δ_P. In Figures 26 and 27 the similar relations τ - δ_R and τ - δ_P to Figures 24 and 25 are shown for the analysis cases D3, E, and F (d = 600 mm). In Figures 28-30 the crack strain at the maximum load as in Figure 21 is plotted and compared with the cracking pattern after failure in the experiment. The distributed crack lines near the loading and supporting plates are considered to represent shear-compressive damage of concrete.

It is obvious that the maximum load is obtained after the shear-compressive failure localizes near the loading plate in the all analysis cases. Since in the post-peak regime for the analysis cases D1, E, and F the shear-compressive failure localizes only near the loading plate and the unloading deformation in the other area is dominant, the response δ_R reveals snapback. However, the snapback behavior is not observed in the response δ_P for all the analysis cases. In the earlier loading stage the shear response of the analysis case E, in which the uniform fixed

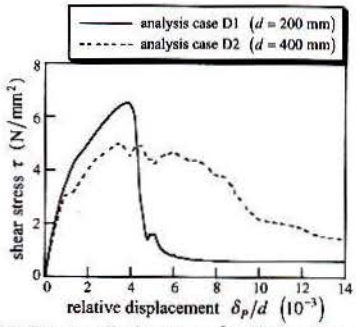

Figure 25. Relative displacement δ_P (d = 200 and 400 mm)

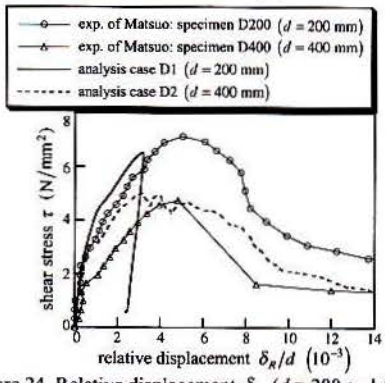

Figure 24. Relative displacement δ_R (d = 200 and 400 mm)

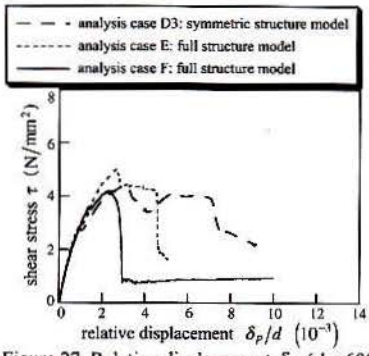

Figure 27. Relative displacement δ_P (d = 600 mm)

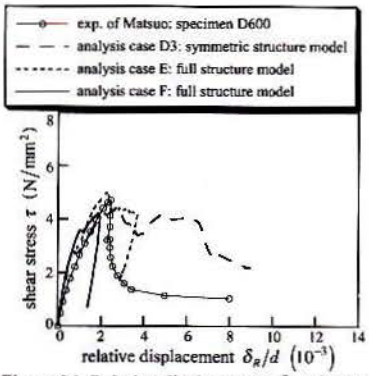

Figure 26. Relative displacement δ_R (d = 600 mm)

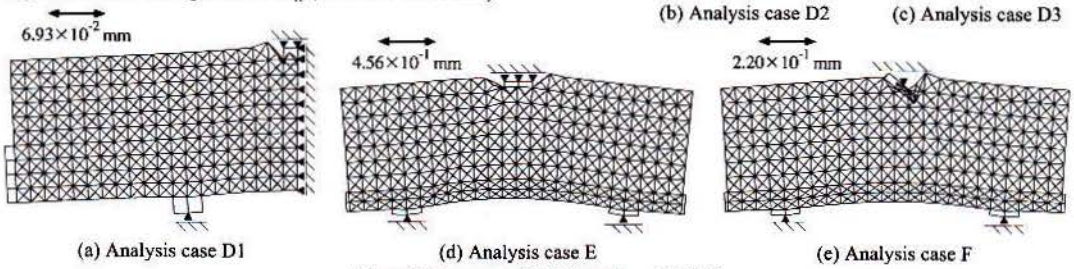

(a) Analysis case D1 (d) Analysis case E (e) Analysis case F

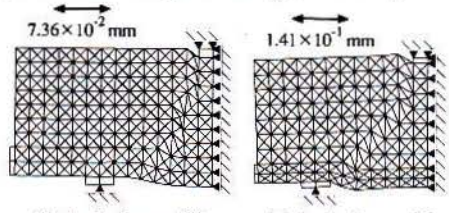

(b) Analysis case D2 (c) Analysis case D3

Figure 23. Incremental deformation at $2V_u/3$

displacement load is applied to the full structure model, is almost identical to the analysis case D3 of symmetric structure model. However, when the shear crack in the left span propagates further a bifurcation from a symmetric to an unsymmetrical fracture mode occurs in the analysis case E. Then the difference of shear response between the analysis cases D3 and E begins increasing gradually. The crack strain distribution of left and right spans is similar and approximately symmetric at the maximum load in the analysis case F. On the other hand the crack profile of the analysis case E is different between the left and right spans, which indicates that an unsymmetrical fracture mode is dominant.

Figure 31 is stress-strain responses of the elements *a* and *b* (Figure 10) in the analysis cases E and F. Very similar softening fracture responses occur in both elements *a* and *b* for the analysis case E while in the analysis case F the unloading responses take place at the maximum load in the element *a* of the left span and the softening fracture responses occur in the element *b* of the right span. In the analysis case F the shear-compressive failure localization near the right end of loading plate induces the rotation of the loading plate, which intensifies the unsymmetrical fracture mode. The loading boundary condition has an important influence on the bifurcation to the unsymmetrical fracture mode and the fracture localization in reinforced concrete deep beams. In the experimental study of Matsuo as well as Niwa the details of the loading boundary conditions such as the arrangement of spherical seat and load cell were not

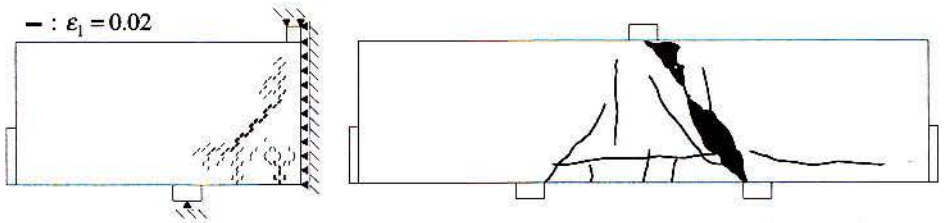

Figure 28. Crack strain at maximum load in analysis case D1, and cracking pattern after failure in the test (d = 200 mm)

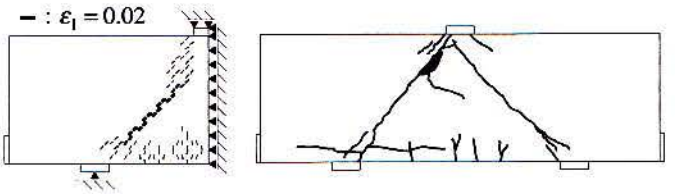

Figure 29. Crack strain at maximum load in analysis case D2, and cracking pattern after failure in the test (d = 400 mm)

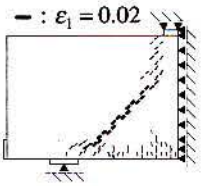

(a) Analysis case D3

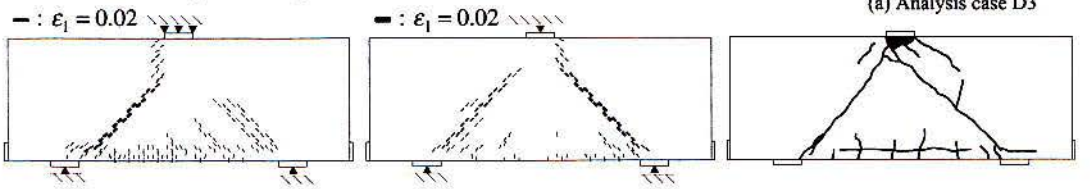

(b) Analysis case E (c) Analysis case F (d) Cracking pattern after failure in the test

Figure 30. Crack strain at maximum load in analysis cases D3, E, and F, and cracking pattern after failure in the test (d = 600 mm)

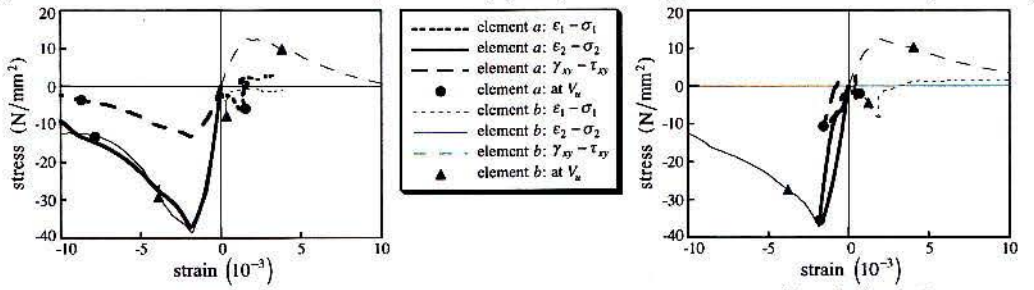

(a) Analysis case E (b) Analysis case F

Figure 31. Stress-strain responses in analysis cases E and F (d = 600 mm)

clarified, which are related to the rotation degree of freedom and the deformation of the loading plate. Therefore, it was difficult to pursue further the issue of the loading boundary conditions in the present analysis.

A detailed examination reveals that the rotation of principal direction within the elements *a* and *b* is too large to be ignored. Since the MESP Model has an important advantage that the model is rationally applicable to the stress and strain conditions in which the principal direction rotates, it seems that the advantage of the model results in the present reasonable simulation with accuracy.

Figure 32 shows the minimum principal strain distribution at the maximum load in the analysis case E. From Figure 32 and the comparison between Figures 30 (b) and (c) the uniform displacement load at the loading plate is considered to make the shear crack band occur at a lower position in the web, which results in widening of the concrete compressive strut between the loading and supporting plates and it enhances the shear capacity. It is worth notice that the analysis case D3 with the symmetric structure model brings about different results from the analysis case E with full structure model in terms of not only the shear strength but also the failure mode and the post-peak response (ductility). An assumption of symmetric structure model has to be paid great attention for simulation of reinforced concrete deep beams.

In Figure 33 the size effect of shear strength obtained in the analysis cases D, E, and F is compared with experimental test data of Matsuo and Walraven

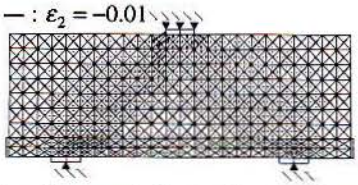

Figure 32. minimum principal strain at maximum load in analysis case E

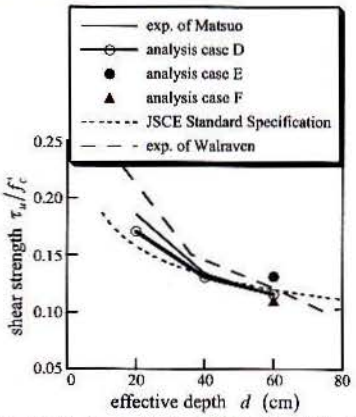

Figure 33. Size effect on shear strength (a/d = 1.0)

(Walraven & Lehwalter 1994) along with the design equation of the Japan Society of Civil Engineers Standard Specification. As in the analysis cases A, B, and C the analysis method using the MESP and EMPC Models can predict the size effect on shear strength of reinforced concrete deep beams with accuracy.

4 CONCLUSIONS

The Multi Equivalent Series Phase Model and the Enhanced Microplane Concrete Model can provide good prediction of experimental results of reinforced concrete deep beams on the cracking, shear-compressive failure localization, failure mechanism, deformation, shear strength, and its size effect. The loading boundary condition and the geometrical unsimilarity in beam shape other than in the shear span are shown to have important influence on not only the shear strength but also the failure mode and post-peak behavior.

5 REFERENCES

Hasegawa, T. 1995. Enhanced microplane concrete model. In F. H. Wittmann (ed.), *Fracture Mechanics of Concrete Structures*: 857-870. Friburg: AEDIFICATIO Publishers.

Hasegawa, T. 1998. Multi equivalent series phase model for nonlocal constitutive relations of concrete. In H. Mihashi & K. Rokugo (eds), *Fracture Mechanics of Concrete Structures*: 1043-1054. Friburg: AEDIFICATIO Publishers.

Hasegawa, T. 1999. Size effect analysis of reinforced concrete deep beam using Multi equivalent series phase model. *Proceedings of the 54th annual conference of JSCE* 5: 588-589.

Matsuo, M. 2001. Shear tests of reinforced concrete deep beams. *JCI committee report on test method for fracture property of concrete*. Tokyo: JCI.

Niwa, J. 1983. *Shear load carrying mechanism of reinforced concrete members like deep beam, Ph.D. thesis, The University of Tokyo*. Tokyo.

Shima, H., Chou, L., & Okamura, H. 1987. Micro and macro models for bond in reinforced concrete. *Journal of the Faculty of Engineering, The University of Tokyo (B)* 39(2): 133-194.

Walraven, J. & Lehwalter, N. 1994. Size effects in short beams loaded in shear. *ACI Structural Journal* 91(5): 585-593.

Yoshitake, K. & Hasegawa, T. 2000. Parametric study for size effect of reinforced concrete deep beam on shear strength. *Proceedings of the 55th annual conference of JSCE* 5: V-523.